Second-order nonlinear optical susceptibilities in asymmetric coupled quantum wells

2008 J. Phys.: Condens. Matter 20 255214

(http://iopscience.iop.org/0953-8984/20/25/255214)

IOP PUBLISHING JOURNAL OF PHYSICS: CONDENSED MATTER

J. Phys.: Condens. Matter **20** (2008) 255214 (6pp) doi:10.1088/0953-8984/20/25/255214

Second-order nonlinear optical susceptibilities in asymmetric coupled quantum wells

Bin Chen, Kang-Xian Guo[1], Zuo-Lian Liu, Rui-Zhen Wang, Yun-Bao Zheng and Bin Li

Department of Physics, College of Physics and Electronic Engineering, Guangzhou University, Guangzhou 510006, People's Republic of China

E-mail: axguo@sohu.com

Received 28 December 2007, in final form 25 March 2008
Published 21 May 2008
Online at stacks.iop.org/JPhysCM/20/255214

Abstract

The second harmonic generation (SHG) in the asymmetric coupled quantum wells (ACQWs) is studied theoretically for different widths of the right-well and the barrier. The analytical expression of the SHG susceptibility is deduced by using the compact density matrix approach and the iterative method. Numerical calculations are presented for typical GaAs/$Al_xGa_{1-x}As$ ACQWs. The results show that the calculated SHG susceptibility in this coupled system can reach a magnitude of 10^{-5} m V^{-1}, 1–2 orders higher than that in single quantum systems. Moreover, the SHG susceptibilities are not monotonic functions of the widths of the right-well and the barrier, but have complex relationships with them. The calculated results also reveal that by adjusting the widths of the right-well and the barrier respectively, a set of optimal structural parameters can be found for obtaining a strong SHG susceptibility.

1. Introduction

In the past few years, nonlinear optical properties in the low-dimensional semiconductor quantum systems, such as quantum wells, quantum wires, and quantum dots, have attracted much attention in both practical applications and theoretical research. This is because the nonlinear effects can be enhanced dramatically in these low-dimensional quantum systems over those in bulk materials due to the existence of a quantum-confinement effect. In addition the fast development of growing technologies such as molecular-beam epitaxy and metal-organic chemical vapor deposition has also accelerated research in this area. Among the nonlinear optical properties, more attention has been paid to the second-order ones, such as second harmonic generation [1–12], optical rectification [13–16], the electro-optic effect [17] and so on. Because the magnitudes of the second-order nonlinear susceptibility are usually stronger than those of higher-order ones, studies in this area have more significance for the practical applications.

[1] Author to whom any correspondence should be addressed.

It is interesting that the second-order nonlinear susceptibility vanishes in symmetric systems, because optical transitions between the electronic states with the same parity are not allowed. Therefore, to obtain a strong second-order optical nonlinearity, it is necessary to break the inversion symmetry of the quantum systems. Some authors [5, 9, 14, 16] have researched the second-order nonlinear effect in symmetric quantum systems with incident electric field. Some others have also studied the same effects in some asymmetric single quantum systems, such as in semi-parabolic quantum systems [4, 13, 15, 17], in asymmetric step wells [1–3] and so on. However, only a few authors [6–8, 18–23] have focused attention on researches into the nonlinear optical effects of asymmetric coupled quantum systems, and a systematic study of the second-order effects of optical nonlinearity in these systems is still lacking. So the research in this field is still important both theoretically and for practical applications.

In this paper, the second harmonic generation (SHG) susceptibility in the GaAs/$Al_xGa_{1-x}As$ asymmetric coupled quantum wells (ACQWs) is investigated. The construction of this asymmetric system is shown in figure 1. We keep the width of the left-well (denoted by the symbol W_L) unchanged, and restrict our attention to the influence of the widths of the

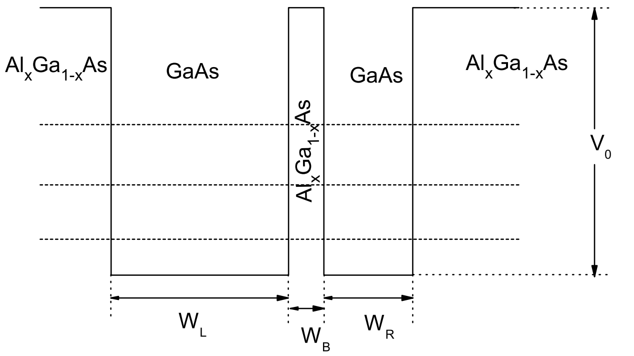

Figure 1. Schematic diagram for electronic confined potential profile and the first three bound energy levels in an asymmetric coupled GaAs/Al$_x$Ga$_{1-x}$As quantum well.

right-well and the barrier (denoted by the symbols W_R and W_B, respectively) on the SHG susceptibility.

This paper is organized as follows. In section 2, the Hamiltonian, relevant eigenstates and eigenenergies are discussed in the GaAs/Al$_x$Ga$_{1-x}$As ACQWs, and the analytical expression of the SHG susceptibility is deduced by the compact density matrix approach and an iterative method. In section 3, numerical calculations for typical GaAs/Al$_x$Ga$_{1-x}$As ACQWs are performed, and the SHG susceptibility as a function of W_R and W_B is plotted and analyzed in detail. Finally, brief conclusions are given in section 4.

2. Theory

Firstly, let us discuss the eigenstates and the eigenenergies in ACQWs. For simplicity, we suppose an idealized ACQW heterostructure model, where we neglect band nonparabolicity and variable effective mass.

In the effective mass approximation, the electron Hamiltonian in this ACQW is well described by

$$H = -\frac{\hbar^2}{2m^*}\left[\frac{\partial^2}{\partial x^2} + \frac{\partial^2}{\partial y^2} + \frac{\partial^2}{\partial z^2}\right] + V(z), \quad (1)$$

with

$$V(z) = \begin{cases} V_0, & z < -(W_L + W_B/2), \\ & -W_B/2 \leqslant z \leqslant W_B/2, \\ & z > W_B/2 + W_R \\ 0, & \text{elsewhere}. \end{cases} \quad (2)$$

Here z represents the growth direction of this quantum well, $\hbar$ is Planck's constant, m^* is the effective mass of the conduction-band, and V_0 is the profile of the conduction-band potential in this quantum well, respectively. By solving the Schrödinger equation $H\psi_{n,\mathbf{k}}(\mathbf{r}) = e_{n,\mathbf{k}}\psi_{n,\mathbf{k}}(\mathbf{r})$, the eigenfunctions $\psi_{n,\mathbf{k}}(\mathbf{r})$ and the eigenenergies $e_{n,\mathbf{k}}$ are given by

$$\psi_{n,\mathbf{k}}(\mathbf{r}) = \varphi_n(z)u_c(\mathbf{r})e^{i\mathbf{k}_\parallel\cdot\mathbf{r}_\parallel}, \quad (3)$$

and

$$e_{n,\mathbf{k}} = E_n + \frac{\hbar^2}{2m^*}|\mathbf{k}_\parallel|^2, \quad (4)$$

respectively. Here, $\mathbf{k}_\parallel$ and $\mathbf{r}_\parallel$ are the wavevector and coordinate in the xy plane and $u_c(\mathbf{r})$ is the periodic part of the Bloch function in the conduction-band at $\mathbf{k} = 0$. $\varphi_n(z)$ and E_n are the solutions of the one-dimensional Schrödinger equation

$$H_0\varphi_n(z) = E\varphi_n(z), \quad (5)$$

where H_0 is the z component of the whole Hamiltonian H, and is given by

$$H_0 = -\frac{\hbar^2}{2m^*}\frac{d^2}{dz^2} + V(z). \quad (6)$$

By solving equation (5), the bound states can be given as follows,

$$\varphi(z) = \begin{cases} A\exp\{kz\} \\ B_1\cos\{k'z\} + B_2\sin\{k'z\} \\ C_1\exp\{-kz\} + C_2\exp\{kz\} \\ D_1\cos\{k'z\} + D_2\sin\{k'z\} \\ G\exp\{-kz\} \end{cases} \quad (7)$$

with the wavevectors given by $k = \sqrt{2m^*(V_0 - E)}/\hbar$ and $k' = \sqrt{2m^*E}/\hbar$, where E is the corresponding eigenenergy, and $A, B_1, B_2, C_1, C_2, D_1, D_2$ and G are the normalized coefficients of the wavefunction. All of these normalized coefficients and the eigenenergy E can be numerically solved by the standard boundary condition of the electronic bound state.

Next, the formula of the SHG susceptibility in ACQWs will be deduced by the compact density matrix method and an iterative procedure. Assuming a monochromatic incident electromagnetic field $E(t) = \tilde{E}\exp\{-i\omega t\} + \tilde{E}\exp\{i\omega t\}$ is applied to the system with a polarization vector normal to the quantum wells, the evolution of the one-electron density matrix ρ is given by the time-dependent Schrödinger equation

$$\frac{\partial\rho_{ij}}{\partial t} = \frac{1}{i\hbar}\left[H_0 - qzE(t), \rho\right]_{ij} - \Gamma_{ij}(\rho - \rho^{(0)})_{ij}, \quad (8)$$

where H_0 is the Hamiltonian for this system without the incident field $E(t)$, q is the electronic charge, $\rho^{(0)}$ is the unperturbed density matrix and Γ_{ij} is the relaxation rate. For simplicity, we will assume $\Gamma_{ij} = \Gamma_0 = 1/T_0$ for $i \neq j$. Equation (8) is solved using the usual iterative method [1, 5]:

$$\rho(t) = \sum_n \rho^{(n)}(t) \quad (9)$$

with

$$\frac{\partial\rho_{ij}^{(n+1)}}{\partial t} = \frac{1}{i\hbar}\left\{\left[H_0, \rho^{(n+1)}\right]_{ij} - i\hbar\Gamma_{ij}\rho_{ij}^{(n+1)}\right\} - \frac{1}{i\hbar}\left[qz, \rho^{(n)}\right]_{ij}E(t). \quad (10)$$

The electronic polarization of the square quantum wells can be expanded as equation (9). We will restrict ourselves to considering the first two orders, i.e.

$$P(t) = \varepsilon_0\left(\chi_\omega^{(1)}\tilde{E}e^{i\omega t} + \chi_{2\omega}^{(2)}\tilde{E}^2e^{2i\omega t}\right) + \text{c.c.} + \varepsilon_0\chi_0^{(2)}\tilde{E}^2, \quad (11)$$

where $\chi^{(1)}_{\omega}$, $\chi^{(2)}_{2\omega}$ and $\chi^{(2)}_{0}$ denote the linear, second harmonic generation, and optical rectification susceptibility, respectively. ε_0 is the vacuum permittivity. The electronic polarization of the nth order is given by

$$P^{(n)}(t) = \frac{1}{S}\,\mathrm{Tr}(\rho^{(n)}qz), \tag{12}$$

where S is the area of interaction. By using the same compact density matrix approach and the iterative procedure as [1] and [16], the expression of SHG susceptibility per unit area can be deduced finally, and is given as:

$$\chi^{(2)}_{2\omega} = \frac{q^3}{\varepsilon_0}\sum_i\sum_j \frac{1}{(2\hbar\omega + E_{ji}) - \mathrm{i}\hbar\Gamma_{ji}} \times \sum_k \mu_{ij}\mu_{jk}\mu_{ki}\left[\frac{\rho_i - \rho_k}{(\hbar\omega + E_{ki}) - \mathrm{i}\hbar\Gamma_{ki}} - \frac{\rho_k - \rho_j}{(\hbar\omega + E_{jk}) - \mathrm{i}\hbar\Gamma_{jk}}\right], \tag{13}$$

where $E_{lm} = (E_l - E_m)$ is the transition energy between the lth and the mth sub-bands, $\mu_{lm} = \langle l|z|m\rangle$ is dipole matrix element, $\hbar\omega$ is the incident photon energy and ρ_l is the surface concentration of carriers in the lth sub-band.

In this paper, we mainly focus on the near-double-resonant approximation of the SHG susceptibility, i.e. for $\hbar\omega \approx E_{21} \approx E_{32}$. In this case, the equation (13) can be written simply as

$$\chi^{(2)}_{2\omega} = \frac{q^3\rho_1}{\varepsilon_0}\frac{\mu_{12}\mu_{23}\mu_{31}}{(\hbar\omega - E_{21} - \mathrm{i}\hbar\Gamma_0)(2\hbar\omega - E_{31} - \mathrm{i}\hbar\Gamma_0)}, \tag{14}$$

where ρ_1 has been normalized to a volume density of carriers as [1].

Obviously, the volume SHG susceptibility has a peak value for $2\hbar\omega \approx 2E_{21} \approx E_{31}$ given by

$$\chi^{(2)}_{2\omega,\max} = \frac{q^3\rho_1}{\varepsilon_0}\frac{\mu_{12}\mu_{23}\mu_{31}}{\hbar^2\Gamma_0^2}. \tag{15}$$

3. Results and discussions

In order to find the relationships between the SHG susceptibility and the parameters of size structure in the GaAs/Al$_x$Ga$_{1-x}$As ACQWs, the numerical calculations are carried out in the present section. The parameters adopted in our calculations are as follows [4, 5, 22]: $m^* = 0.067m_0$ (m_0 is the free -electron mass), $V_0 = 228$ meV (corresponding Al concentration $x = 0.3$), $\rho_1 = 5\times10^{24}$ m^{-3}, $T_0 = 0.14$ ps, and $\varepsilon_0 = 8.85\times10^{-12}$ F m^{-1}.

In figure 2(a), the SHG susceptibility $|\chi^{(2)}_{2\omega}|$ is plotted as a function of the incident photon energy $\hbar\omega$ for seven different right-well widths, $W_R = 3$, 4, 4.5, 4.791, 5, 5.5 and 7.5 nm, while W_L and W_B are kept at 10 and 2 nm, respectively. It can be seen easily from the figure that, firstly, the strength of the SHG susceptibility in the ACQWs can reach the magnitude of 10^{-5} m V^{-1}, which is 1–2 orders higher than that in single quantum systems [5, 12]. This large SHG effect is primarily attributed to the strong coupling between the double wells. Secondly, the SHG susceptibilities are not a monotonic function of W_R. To make this feature clearer, we have plotted figure 2(b), which presents the SHG susceptibility $|\chi^{(2)}_{2\omega}|$ as a function of W_R for $W_L = 10$ nm, $W_B = 2$ nm and $\hbar\omega_0 = 49.5$ meV. The two figures show that if W_L and W_B are fixed, W_R plays an important role in getting a large $|\chi^{(2)}_{2\omega}|$. Only when W_R is chosen as an optimal value, can the largest $|\chi^{(2)}_{2\omega}|$ be obtained. Thirdly, for thicker or thinner right-well, the corresponding peak of $|\chi^{(2)}_{2\omega}|$ becomes wider and even two different peaks may appear. Finally, with the increase of W_R, the peak of $|\chi^{(2)}_{2\omega}|$ has an obvious red-shift. For example, when $W_R = 4$ nm, the corresponding position of the peak is at $\hbar\omega = 52.6$ meV, but when $W_R = 5.5$ nm, the peak's position shifts to 47.2 meV. This behavior can be explained in that with the increase of W_R the quantum-confinement effect to the electron decreases quickly, therefore, the energy levels of this wider system become very close each other, i.e. the energy

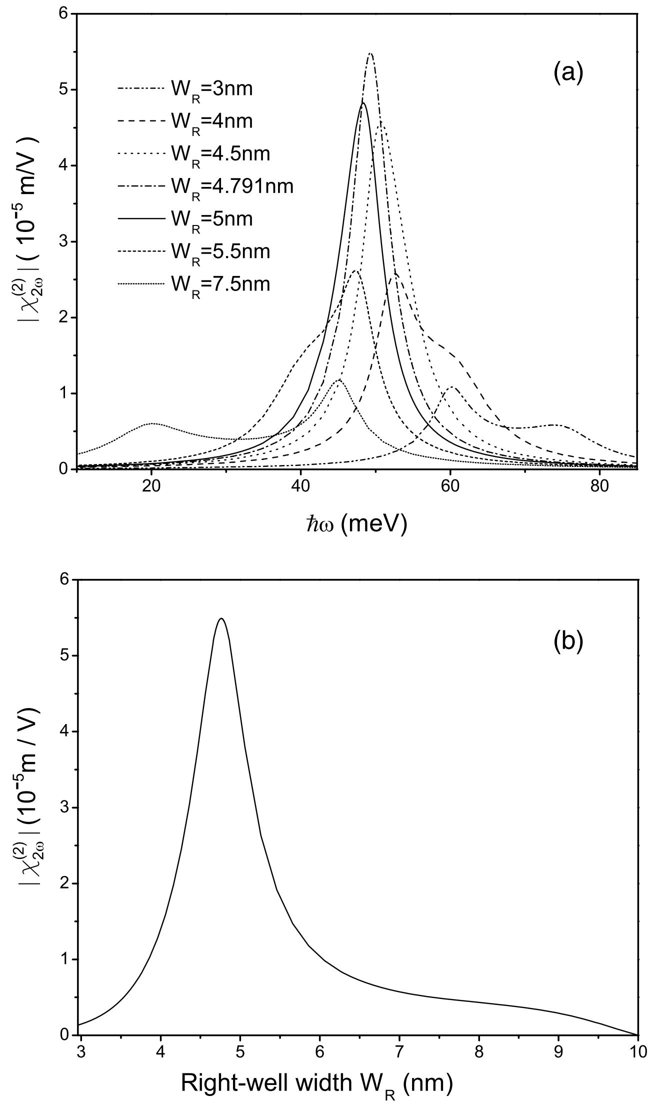

Figure 2. (a) SHG susceptibility $|\chi^{(2)}_{2\omega}|$ as a function of the photon energy $\hbar\omega$ for seven different widths of the right-well, $W_R = 3$, 4, 4.5, 4.791, 5, 5.5 and 7.5 nm, with $W_L = 10$ nm and $W_B = 2$ nm. (b) SHG susceptibility $|\chi^{(2)}_{2\omega}|$ as a function of the right-well width W_R for $W_L = 10$ nm, $W_B = 2$ nm and $\hbar\omega_0 = 49.5$ meV.

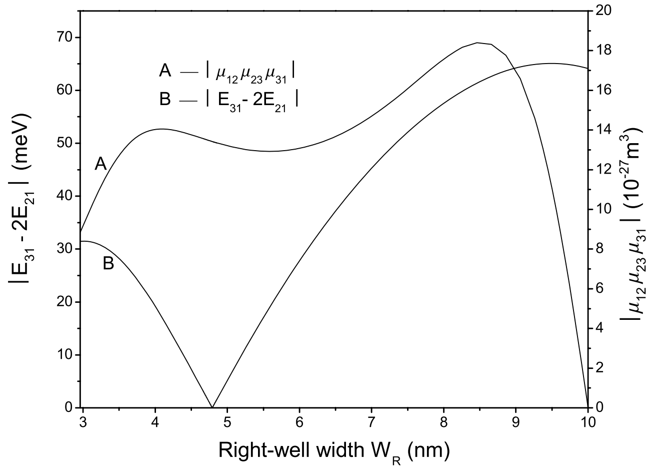

Figure 3. Geometric factor $|\mu_{12}\mu_{23}\mu_{31}|$ of the SHG susceptibility and the difference of the energy intervals $|E_{31} - 2E_{21}|$ as functions of W_R for $W_L = 10$ nm and $W_B = 2$ nm.

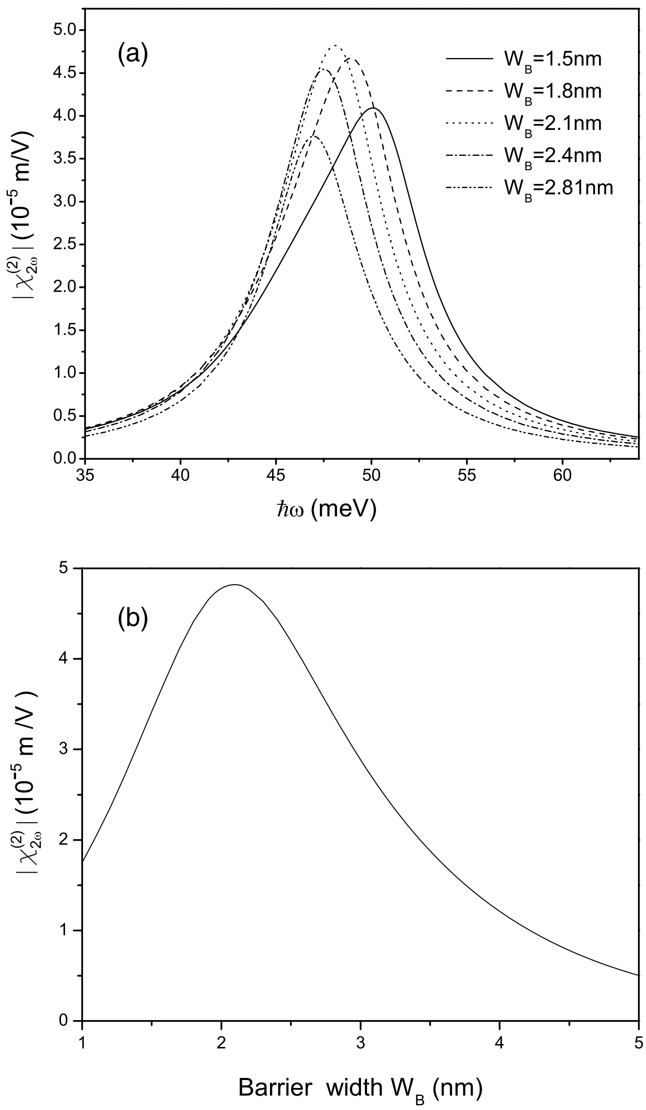

Figure 4. (a) SHG susceptibility $|\chi^{(2)}_{2\omega}|$ as a function of the photon energy $\hbar\omega$ for five different widths of the barrier, $W_B = 1.5$, 1.8, 2.1, 2.4 and 2.81 nm, with $W_L = 10$ nm and $W_R = 5$ nm. (b) SHG susceptibility $|\chi^{(2)}_{2\omega}|$ as a function of the barrier width W_B for $W_L = 10$ nm, $W_R = 5$ nm and $\hbar\omega_0 = 48$ meV.

intervals are reduced, and as a result, the peak of $|\chi^{(2)}_{2\omega}|$ appears at the low-energy direction, i.e. suffers a red-shift.

To understand the above phenomena more clearly, it is useful for us to study the dependence of the geometrical factor $|\mu_{12}\mu_{23}\mu_{31}|$ and the intervals of energies E_{21} and E_{31} on the width of the right-well W_R. Figure 3 shows $|\mu_{12}\mu_{23}\mu_{31}|$ and $|E_{31} - 2E_{21}|$ as a function of W_R respectively, for $W_L = 10$ nm and $W_B = 2$ nm. From this figure, it can be observed that near the double resonant region, i.e. $|E_{31} - 2E_{21}|$ is small enough (corresponding W_R is near to 4.791 nm), the geometric factors are large, and not sensitive to the change of W_R. So it is not surprising to obtain stronger $|\chi^{(2)}_{2\omega}|$ peaks near this region, as shown in figure 2(a). Figure 3 also shows us that, far from the double resonant region, i.e. the right-well is too wide or narrow, there is a great difference between $2E_{21}$ and E_{31}. Therefore, at $\hbar\omega \approx E_{21}$ and $\hbar\omega \approx E_{31}/2$, the $|\chi^{(2)}_{2\omega}|$ will have two different maximum values, respectively. That is to say, the curve of $|\chi^{(2)}_{2\omega}|$ has two different peaks. Moreover, when W_R shifts to the double resonant region gradually, $|E_{31} - 2E_{21}|$ decreases quickly. As a result, the two peaks are closer and closer, and at some values of W_R, they convert to one single wide peak. Close to the double resonant region, because of $|E_{31} - 2E_{21}| \approx 0$, this single peak becomes sharper and sharper.

In figure 4(a), $|\chi^{(2)}_{2\omega}|$ is plotted as a function of the incident photon energy $\hbar\omega$ for five different barrier widths, W_B = 1.5, 1.8, 2.1, 2.4 and 2.81 nm, with $W_L = 10$ and W_R = 5 nm. From this figure, it is clearly observed that the SHG susceptibilities are also not a monotonic function of W_B. This important feature is shown more clearly in figure 4(b), which presents $|\chi^{(2)}_{2\omega}|$ as a function of the barrier width W_B for W_L = 10 nm, $W_R = 5$ nm, and $\hbar\omega_0 = 48$ meV. The two figures show us that there is an optimal barrier width determining the largest $|\chi^{(2)}_{2\omega}|$ while W_L and W_R are kept unchanged. For example, in figure 4(a), when the barrier width is chosen as $W_B = 2.1$ nm, the peak of $|\chi^{(2)}_{2\omega}|$ can reach the maximum value 4.821×10^{-5} m V^{-1}. Moreover, figure 4(a) also shows that the peak of $|\chi^{(2)}_{2\omega}|$ has a small blue-shift with the decrease of W_B. The physical origin of this behavior can be understood in that with the decrease of W_B, the coupling between the left-well and the right-well can be strengthened greatly, which makes the energy levels of this strong coupled quantum system separate from each other, i.e. makes the energy intervals increase. As a result, the peak of $|\chi^{(2)}_{2\omega}|$ shifts towards the high-energy direction, i.e. suffers a blue-shift. However, a more important feature shown in figure 4(a) is that the largest peak value of $|\chi^{(2)}_{2\omega}|$ does not occur at W_B = 2.81 nm, which is the optimal width of the barrier for a double resonant system with W_L = 10 nm and W_R = 5 nm, but at W_B = 2.1 nm. In order to explain this phenomenon, we have plotted figure 5, which presents $|\mu_{12}\mu_{23}\mu_{31}|$ and $|E_{31} - 2E_{21}|$ as functions of W_B for W_L = 10 and W_R = 5 nm. From this figure, it is seen clearly that, when W_B > 1.5 nm, the geometric factor $|\mu_{12}\mu_{23}\mu_{31}|$ has a rapid reduction as W_B increases. Therefore, when we keep the difference between E_{31} and $2E_{21}$ small

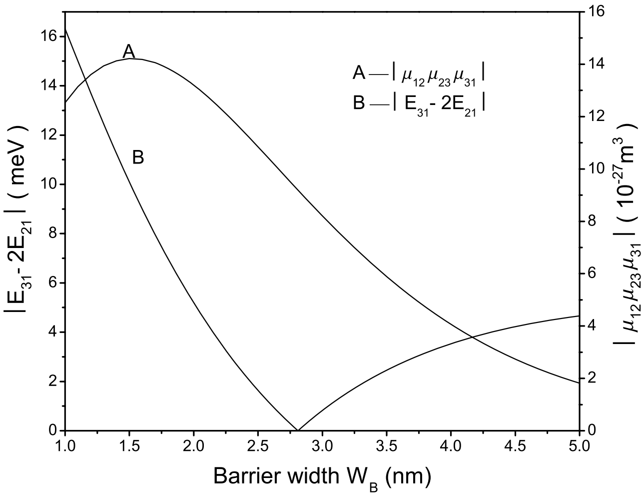

Figure 5. Geometric factor $|\mu_{12}\mu_{23}\mu_{31}|$ of the SHG susceptibility and the difference of the energy intervals $|E_{31} - 2E_{21}|$ as functions of W_B for $W_L = 10$ nm and $W_R = 5$ nm.

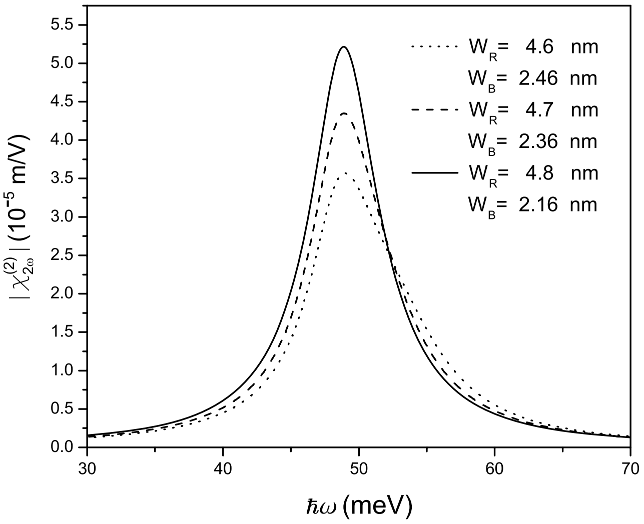

Figure 6. SHG susceptibility $|\chi^{(2)}_{2\omega}|$ as a function of the incident photon energy $\hbar\omega$ for three different sets of W_R and W_B as $(W_R, W_B) = (4.6$ nm, 2.46 nm), (4.7 nm, 2.36 nm) and (4.8 nm, 2.16 nm) with $W_L = 10$ nm.

enough (Under such a condition, $|\chi^{(2)}_{2\omega}|$ mainly depends on the geometric factor.) and choose $W_B < 2.81$, we will get a much larger value of the geometric factor, and accordingly obtain a stronger peak of $|\chi^{(2)}_{2\omega}|$ than that located at $W_B = 2.81$ nm.

Comparing figure 5 with figure 3, we can see that if W_R and W_B are changed in the regions as 4 nm $< W_R <$ 7 nm and 1.5 nm $< W_B <$ 4.5 nm, respectively, W_R primarily influences $|E_{31} - 2E_{21}|$ while W_B primarily affects $|\mu_{12}\mu_{23}\mu_{31}|$. Therefore, we can conclude that if W_L is kept unchanged, by adjusting W_R and W_B in an appropriate region, respectively, an optimal system with an appropriate set of W_R and W_B can be achieved for to obtain the largest value of $|\chi^{(2)}_{2\omega}|$.

Moreover, comparing figure 2(a) with figure 4(a), we can see that increasing W_R can lead to a small red-shift of the peak of $|\chi^{(2)}_{2\omega}|$, while decreasing W_B can result in a small blue-shift of the peak. Therefore, it is expected that the small red-shift will be effectively compensated by the small blue-shift if we keep W_L unchanged and vary W_R (increasing it) and W_B (decreasing it) simultaneously. To confirm this view, we have plotted figure 6 which shows $|\chi^{(2)}_{2\omega}|$ as a function of the incident photon energy $\hbar\omega$ for three different sets of W_R and W_B as $(W_R, W_B) = (4.6$ nm, 2.46 nm), (4.7 nm, 2.36 nm) and (4.8 nm, 2.16 nm) with $W_L = 10$ nm. From this figure we can clearly see that while varying W_R (increasing it) and W_B (decreasing it) simultaneously, some optimal sets of W_R and W_B can be obtained which ensure that the red-shift induced by increasing W_R can be effectively compensated by the blue-shift caused by decreasing W_B.

4. Conclusion

In conclusion, we have presented an efficient study of the second harmonic generation for a typical asymmetric GaAs/Al_xGa_{1-x}As coupled quantum well. The calculations mainly focus on the dependence of $|\chi^{(2)}_{2\omega}|$ on the widths of the right-well and the barrier. Our results show that, the theoretical value of $|\chi^{(2)}_{2\omega}|$ can reach a magnitude of 10^{-5} m V^{-1} in this coupled quantum system, which is 1–2 orders higher than that in single quantum systems. We also find that the SHG susceptibility is not a monotonic function of W_R or W_B, but has complicated relationships with them. And the most important feature is that we find the double-photon-resonant system (i.e. $E_{21} = E_{32}$) is not always the best system for obtaining the largest value of $|\chi^{(2)}_{2\omega}|$. Based on this double-photon-resonant system, we can get a much stronger peak of $|\chi^{(2)}_{2\omega}|$ by adjusting W_B properly. Moreover, our results also reveal that if W_L is fixed but W_R and W_B is changed in an appropriate region, W_R primarily influences the energy levels of this coupled system, while W_B primarily affects the geometric factor. Therefore, it is expected that an optimum system will be achieved by choosing appropriate values of W_R and W_B to obtain a stronger $|\chi^{(2)}_{2\omega}|$. More importantly, the calculated results also show us that the small red-shift induced by increasing W_R can be effectively compensated by the small blue-shift caused by decreasing W_B simultaneously, while keeping W_L unchanged. Finally we hope these important conclusions can make a great contribution to the experimental studies, have a significant influence on improvements of optical devices, such as ultrafast optical switches, and open up new opportunities for practical exploration of the quantum-size effect on devices.

Acknowledgments

This work is supported by the National Natural Science Foundation of China (under Grant No. 60478010) and the Science and Technology Committee of Guangdong Province (under Grant Nos 2007B010600061 and 07001899).

References

[1] Rosencher E and Bois P 1991 *Phys. Rev.* B **44** 11315
[2] Sedrakian D M, Khachatrian A Z, Andresyan G M and Badalyan V D 2004 *Opt. Quantum Electron.* **36** 893

[3] Indjin D, Mirčetić A, Ikonić Z, Milanović V and Todorović G 1999 *Physica* E **4** 119
[4] Zhang C J and Guo K X 2006 *Physica* E **33** 363
[5] Zhang L and Xie H J 2003 *Phys. Rev.* B **68** 235315
[6] Zhang L, Chi Y M and Shi J-J 2007 *Phys. Lett.* A **366** 256
[7] Park T-I, Gumbs G and Chen Y C 1999 *J. Appl. Phys.* **86** 1467
[8] Jiang Y Q, Xu J H, Wang W J, Lu X Z, Liu X, Wang G M and Li F M 2001 *Phys. Rev.* B **63** 125308
[9] Guo K X and Chen C Y 1996 *Solid State Commun.* **99** 363
[10] Liu J L, Bai Y C and Xiong G G 2004 *Physica* E **23** 70
[11] Sauvage S, Boucaud P, Brunhes T, Glotin F, Prazeres R, Ortega J M and Gérard J M 2001 *Phys. Rev.* B **63** 113312
[12] Li B, Guo K X, Zhang C J and Zheng Y B 2007 *Phys. Lett.* A **367** 493
[13] Karabulut İ and Safak H 2005 *Physica* B **368** 82
[14] Guo K X and Chen C Y 1995 *J. Phys.: Condens. Matter* **7** 6583
[15] Baskoutas S, Paspalakis E and Terzis A F 2006 *Phys. Rev.* B **74** 153306
[16] Guo K X and Gu S W 1993 *Phys. Rev.* B **47** 16322
[17] Yu Y B and Guo K X 2003 *Physica* E **18** 492
[18] Bedoya M and Camacho A S 2005 *Phys. Rev.* B **72** 155318
[19] Chen Y J, Koteles E S, Elman B S and Armiento C A 1987 *Phys. Rev.* B **36** 4562
[20] Yuh P F and Wang K L 1988 *Phys. Rev.* B **38** 8377
[21] Santiago R B and Guimarães L G 2002 *Solid-State Electron.* **46** 89
[22] Ozturk E and Sokmen I 2007 *Superlatt. Microstruct.* **41** 36
[23] Goldoni G 2001 *J. Appl. Phys.* **89** 1755